*informatics*

MDPI

*Article*

# An Intelligent Temporal Framework for Interval Prediction of Concrete Dam Deformation

**Feng Han, Chongshi Gu *, Pei Liu and Xinran Cui**

College of Water Conservancy and Hydropower Engineering, Hohai University, Nanjing 210098, China; hfsgghz@126.com or 190802020007@hhu.edu.cn (F.H.); 250402020001@hhu.edu.cn (P.L.); cuixinran_hhu@163.com (X.C.)

* Correspondence: csgu@hhu.edu.cn; Tel.: +86-13809043532

**Abstract**

The inherent uncertainty of concrete dam systems, together with the complex influence of environmental loads and measurement noise, makes it difficult for traditional deterministic point prediction models to provide reliable deformation forecasts. In particular, the prediction performance of conventional models is highly dependent on parameter settings, while the uncertainty and potential deviation of future displacement responses are often not fully quantified. To address these limitations, this study proposes an intelligent data-driven prediction framework for dam displacement based on the integration of convolutional neural networks and long short-term memory networks. In the proposed framework, convolutional neural networks are used to extract local feature information from monitoring data, while long short-term memory networks are employed to capture temporal dependencies in displacement sequences. The Black-winged Kite Algorithm is introduced to optimize the key parameters of the integrated multi-level network, thereby improving the accuracy and robustness of point prediction. Furthermore, quantile regression is embedded into the optimized learning framework to construct an interval prediction model for dam deformation, enabling the conditional predictive uncertainty associated with displacement evolution to be quantitatively characterized. The engineering case study and comparative analyses with other models demonstrate that the proposed model achieves improved prediction performance for the investigated monitoring point. The interval prediction results further show that, for the investigated dam and monitoring point, the proposed framework can effectively characterize conditional predictive uncertainty and provide additional information for deformation interpretation and safety assessment. Further studies involving additional monitoring points and dams are required to assess its broader applicability.

**Keywords:** concrete dam; uncertainty deformation; interval prediction; integrated neural network; optimization algorithm for black winged kite

Check for updates

Academic Editor: Sotiris Kotsiantis

Received: 3 July 2026
Revised: 31 August 2026
Accepted: 2 September 2026
Published: 8 September 2026

**Copyright:** © 2026 by the authors. Licensee MDPI, Basel, Switzerland. This article is an open access article distributed under the terms and conditions of the Creative Commons Attribution (CC BY) license.

## 1. Introduction

As a critical component of hydraulic infrastructure, concrete dams play an essential role in flood control, water supply, hydropower generation, and regional development. Their safe operation is closely related to downstream public safety and sustainable water resource management. Regular safety assessment and continuous monitoring provide an important basis for evaluating structural performance, verifying design assumptions, inspecting construction quality, and supporting maintenance decisions [1–3]. In this context,

dam safety monitoring has gradually evolved from the acquisition of single physical quantities into an interdisciplinary information system integrating sensor networks, data acquisition, signal processing, structural mechanics, and intelligent decision-making.

With the development of sensing and information technologies, the monitoring paradigm of concrete dams has shifted from traditional manual inspection and single-point displacement observation to multi-source, multi-parameter, and real-time data-driven assessment. Monitoring information now includes not only deformation, but also stress, seepage, temperature, uplift pressure, environmental loads, and other coupled physical responses [4–7]. These heterogeneous data provide a rich basis for characterizing dam behavior under complex operating conditions. Through effective data integration and analysis, abnormal structural responses can be identified in time, and the evolution trend of dam behavior can be quantitatively assessed. Therefore, intelligent interpretation of monitoring information has become an important issue in dam safety management.

Among various monitoring indicators, displacement is one of the most direct variables reflecting the structural response and safety status of concrete dams [8]. Dam displacement is affected by reservoir water level, temperature variation, time-dependent effects, material creep, foundation deformation, and measurement uncertainty. It usually exhibits nonlinear responses to water level changes, while temperature-induced periodic deformation may account for a considerable part of the annual deformation. As a result, displacement sequences often show temporal dependence, seasonal fluctuation, spatial heterogeneity, and uncertainty, making accurate prediction a challenging task in time-series information modeling.

Quantitative evaluation of dam safety can be achieved by establishing the relationship between deformation monitoring data and influencing factors [9,10]. Traditional dam deformation models mainly include statistical models, deterministic models, and hybrid models. The hydrostatic-temperature-time model and its improved forms have been widely used to decompose dam displacement into water pressure, temperature, and aging components [11–13]. Although these models have clear physical meanings and good interpretability, their performance may be limited when dealing with complex nonlinear relationships, high-dimensional monitoring variables, and non-stationary time-series patterns.

In recent years, machine learning and deep learning methods have provided new solutions for dam displacement prediction. Data-driven models such as back-propagation neural networks, artificial neural networks, extreme learning machines, least-squares support vector machines, and other intelligent algorithms have been applied to dam safety monitoring and deformation prediction [14–16]. Compared with conventional models, these methods have stronger nonlinear mapping and adaptive learning capabilities, and are suitable for extracting latent features from complex monitoring data. From the perspective of informatics, dam displacement prediction can be regarded as a temporal information modeling problem in which historical monitoring sequences, environmental variables, and structural responses are integrated. Therefore, developing an accurate, robust, and interpretable intelligent prediction model is important for improving the information-based management of concrete dam safety. Li et al. improved the Harris Hawk optimization algorithm and combined it with a quasi recurrent neural network to enhance the accuracy of dam deformation prediction [17]. Zhang et al. optimized the parameters of extreme gradient boosting using sparrow search algorithm and established an efficient dam displacement prediction model [18]. Lu et al. used empirical mode decomposition to process the measured data and integrated grey wolf algorithm and long short-term memory network to construct an advanced dam settlement prediction model [19]. Zhang et al. proposed an adaptive optimization based IVM and random forest algorithm to predict

the deformation of concrete dams [20]. Su et al. proposed a method for optimizing the input and parameters of a prediction model using a combination of support vector machines, chaos theory, and particle swarm optimization algorithm, and established a dam safety prediction model [21]. Compared with traditional models, intelligent monitoring models such as neural networks, extreme learning machines, and multi algorithm fusion models have significantly improved prediction accuracy and can more accurately predict the safety status of dams.

However, because the dam displacement prediction is vulnerable to environmental and detection errors, and has periodic and seasonal changes, it is difficult to characterize the uncertainty of the dam displacement by the determined values obtained from the point prediction of a single model, because it cannot describe the probability of occurrence of the predicted values and the range where they may fluctuate [22]. In recent years, interval prediction has demonstrated the advantage of uncertainty prediction in wind power forecasting. In addition to providing point prediction results, it can also depict the fluctuation interval of wind power at a specific confidence level. This feature not only reduces the operational risk of equipment, but also improves the revenue of wind power generation [23]. Therefore, using interval prediction for uncertainty analysis of dam system displacement can effectively quantify the rationality and stability of dam operation risk assessment [24–26]. However, existing studies still present two limitations. First, most intelligent dam-deformation models focus primarily on improving deterministic prediction accuracy, whereas the uncertainty associated with future deformation is rarely quantified within the same learning framework. Second, although feature extraction, temporal learning, metaheuristic optimization, and interval prediction have individually been applied in different forecasting problems, their functional complementarity for dam-deformation prediction has not been sufficiently investigated. In particular, there remains a lack of a unified framework that simultaneously extracts nonlinear correlations among environmental variables, captures the temporal dependence of deformation, adaptively optimizes model hyperparameters, and converts deterministic forecasts into calibrated prediction intervals. To address these gaps, a unified BKA CNN LSTM QR framework is developed in this study for the probabilistic prediction of concrete dam deformation. The methodological contribution is not attributed to the individual development of CNN, LSTM, BKA, or quantile regression, but to the establishment of a coordinated prediction framework in which different limitations of conventional deformation forecasting are addressed by the four components. Specifically, nonlinear local correlations among multiple environmental variables are extracted by CNN, long-term temporal dependencies in dam displacement are captured by LSTM, and the key hyperparameters of the CNN LSTM model are adaptively optimized by BKA, thereby reducing the dependence of prediction performance on empirical parameter selection. Furthermore, quantile regression is incorporated into the optimized learning framework, through which the deterministic prediction model is extended to probabilistic interval prediction and both the expected deformation trend and the associated prediction uncertainty are quantified. In this study, the uncertainty quantified by quantile regression refers specifically to the conditional predictive uncertainty reflected in the response distribution of dam displacement, while epistemic uncertainty associated with the model structure and parameter estimation is not separately quantified. In this way, feature extraction, temporal dependency learning, adaptive parameter optimization, and uncertainty quantification are integrated into a unified framework for dam deformation prediction rather than being treated as independent algorithmic components. The effectiveness of the proposed framework and the contributions of its individual components are further evaluated through benchmark comparisons and ablation experiments in terms of point prediction accuracy, interval reliability, and interval sharpness.

## 2. Basic Theory of Algorithms for Models

### *2.1. BKA Optimization Algorithm*

The Black-winged Kite Optimization Algorithm (BKA) is a recently proposed metaheuristic optimization algorithm introduced by Wang et al. in 2024 [27]. Inspired by the migration and predatory behaviors of black-winged kites, BKA simulates the adaptive search strategies of this species in response to dynamic environmental conditions and varying target positions. By abstracting these biological behaviors into mathematical optimization rules, the algorithm achieves a balance between global exploration and local exploitation, thereby enhancing its ability to search complex solution spaces. Owing to its adaptive search mechanism and robust optimization capability, BKA has potential advantages in addressing nonlinear and high-dimensional optimization problems. The optimization process of BKA mainly consists of three stages.

#### 2.1.1. Population Initialization Stage

Randomly generate an initial population, where the individual position $X_i$ of each black-winged kite represents a potential solution in the solution space:

$$X_i = X_{\min} + rand(0,1)(X_{\max} - X_{\min}) \tag{1}$$

where *rand* is a random value between 0 and 1, and $X_{\min}$ and $X_{\max}$ are the boundaries of the search space.

#### 2.1.2. Phase of Attack

As a predator of small grassland mammals and insects, the black-winged kite usually analyzes the current wind speed to control its flight status during flight, and can observe prey and launch attacks in the air. This strategy includes different attack behaviors for global exploration and search, and its mathematical model is

$$\boldsymbol{X}(t+1) = \begin{cases} \boldsymbol{X}(t) + n(1+\sin(r)) \times X(t) & p < r \\ \boldsymbol{X}(t) + n \times (2r-1) \times \boldsymbol{X}(t) & \text{else} \\ n = 0.05 \times exp(-2 \times t/T)^2 \end{cases} \tag{2}$$

where $p$ is a constant, $T$ is the total number of iterations, and $t$ is the number of completed iterations.

#### 2.1.3. Migration Stage

Bird migration is a complex behavior influenced by environmental factors such as climate and food supply. To adapt to seasonal changes, many birds migrate from the north to the south in winter to obtain better living conditions and resources. Migration is usually led by leaders, whose navigation skills are crucial to the success of the team. If the fitness value of the current population is lower than that of the random population, the leader will abandon leadership and join the migrating population, indicating that it is not suitable for leading the population forward. On the contrary, if the fitness value of the current population is greater than that of the random population, it will guide the population to reach its destination. The BKA incorporates a leader strategy based on this characteristic, and by selecting suitable leaders, it can effectively ensure that the population migrates to a resource-rich place. The relevant update formula is as follows:

$$\boldsymbol{X}(t+1) = \begin{cases} \boldsymbol{X}(t) + C(0,1) \times \left(\boldsymbol{X}(t) - L_t^j\right) & F_i < F_{ri} \\ \boldsymbol{X}(t) + C(0,1) \times \left(L_t^j - \mathrm{m} \times \boldsymbol{X}(t)\right) & \text{else} \\ m = 2 \times sin(r + \pi/2) \end{cases} \tag{3}$$

where $F_i$ is the fitness value of the current position; $F_{ri}$ is the fitness value for random positions; $C(0,1)$ is a random number generated in the Cauchy distribution.

BKA is employed to optimize the key hyperparameters of the CNN LSTM model because the search space contains different combinations of network structure and training parameters. Its population-based search provides a flexible balance between global exploration and local exploitation for identifying effective parameter combinations. In this study, its optimization performance is further evaluated against DBO and POA under the same search space, population size, iteration number, validation dataset, and fitness function.

### 2.2. CNN-LSTM Integrated Model

A Convolutional Neural Network (CNN) is a feedforward neural network mainly composed of convolutional layers that extract data feature information, pooling layers that filter and compress the feature information extracted by the convolutional layers, and fully connected layers that aggregate and integrate the information processed by the previous layers [28]. The structure diagram of CNN is shown as Figure 1.

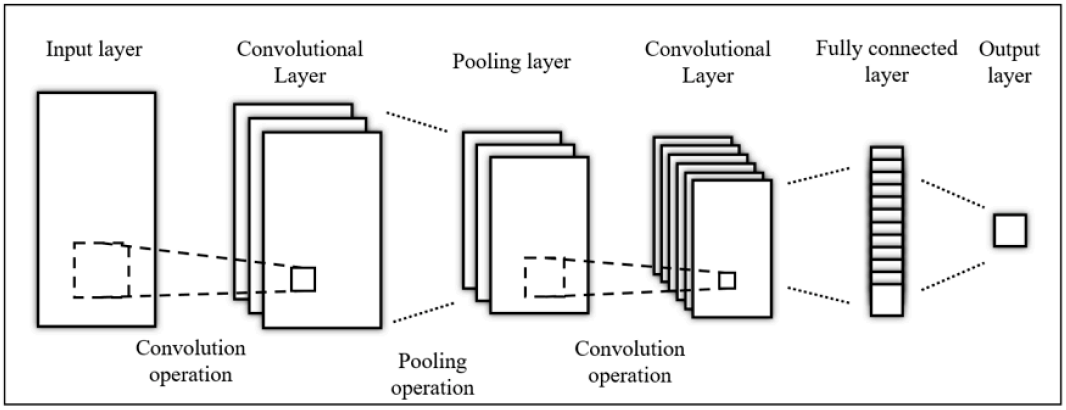



**Figure 1.** Structure diagram of CNN.

Convolutional neural networks (CNNs) are widely used for feature extraction because local patterns in input data can be identified through convolution operations. A typical CNN consists mainly of convolutional layers, pooling layers, and fully connected layers, as illustrated in Figure 1. In the present study, the displacement and environmental variables are organized as temporally ordered one-dimensional sequences. Therefore, a one dimensional CNN is adopted to extract local nonlinear features from adjacent observations before the extracted features are transferred to LSTM for temporal dependency learning [29]. For an input sequence ($X(t)$), the convolution operation can be expressed as

$$C(t) = \sum_{a=0}^{k-1} X(t+a) \cdot K(a) + b \tag{4}$$

where $C(t)$ is the output of the convolutional layer at time step $t$; $X(t)$ is the value of the input sequence at time step $t$; $K(a)$ is the weight of the convolution kernel at position $a$; $k$ is the size of the convolution kernel; $b$ is the bias term.

Long short-term memory (LSTM) is a special type of recurrent neural network that performs better in time series data processing and prediction compared to ordinary RNNs [30–32]. It can effectively solve some key problems in traditional RNNs, including gradient explosion, gradient vanishing, and long-term dependencies. The network structure of LSTM consists of multiple repeated unit modules, each of which contains three gates (forget gate, input gate, output gate). The structure diagram of LSTM is shown as Figure 2.

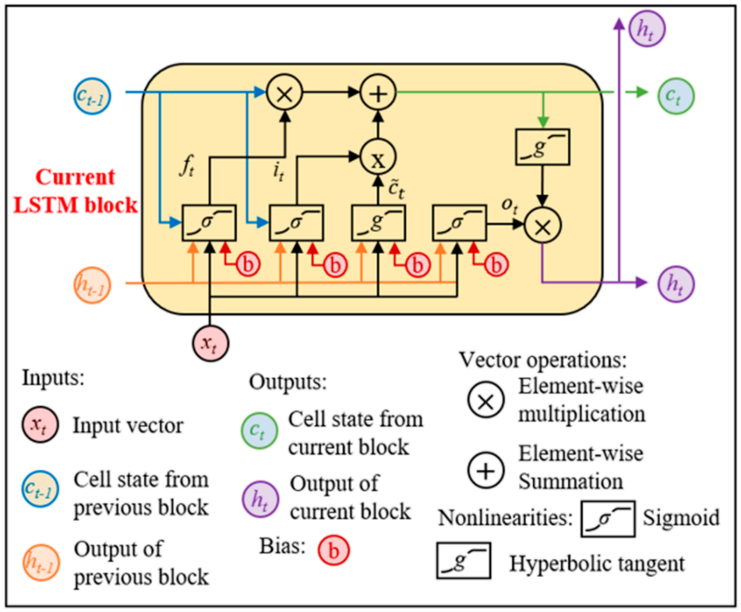



**Figure 2.** Structure diagram of LSTM.

In the proposed framework, CNN and LSTM are sequentially integrated rather than independently applied. The environmental variables, including water pressure, temperature, and aging factors, together with historical deformation information, are first organized as model inputs. The one-dimensional CNN is used to extract local nonlinear features from the temporally ordered displacement and environmental input sequences. The extracted features are then transferred to the LSTM layer to capture longer term temporal dependencies in dam deformation. In this way, CNN and LSTM provide complementary capabilities for local feature extraction and temporal dependency learning, respectively. The resulting hidden features are finally mapped to the predicted dam displacement through a fully connected layer. In this way, the local feature extraction capability of CNN and the temporal dependency learning capability of LSTM are combined within a unified prediction architecture. Based on this, this article first uses CNN to extract the feature vector of dam displacement, and then inputs it into the LSTM network. Recurrent training is carried out in the LSTM network, through which the local feature extraction ability of CNN and the temporal dependency learning ability of LSTM are effectively combined to construct a CNN LSTM integrated model. The model structure is shown in Figure 3.

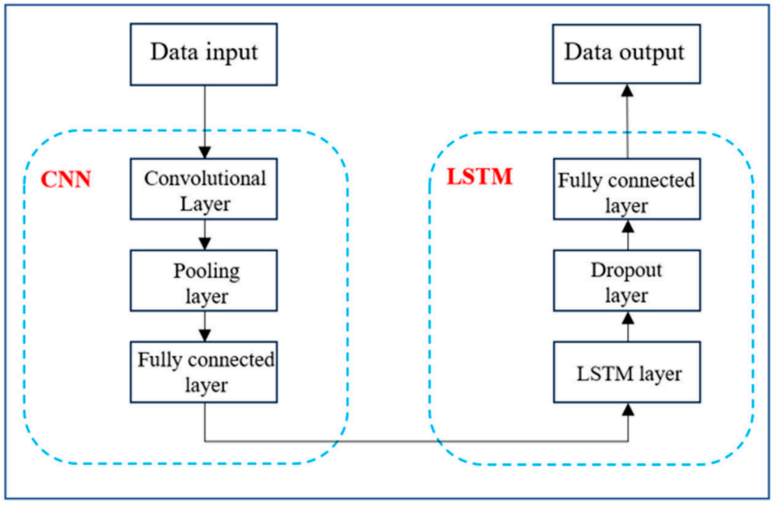



**Figure 3.** Structure diagram of CNN-LSTM model.

## 3. Interval Prediction Model for Deformation of Concrete Dam

The BKA optimization algorithm was used to optimize the parameters of the CNN-LSTM model, and a dam displacement prediction model (BKA-CNN-LSTM point prediction model) was established. The point prediction of dam displacement in actual engineering was carried out to verify the superiority of the proposed model. Quantile regression is adopted to characterize the conditional predictive uncertainty of dam displacement at specified confidence levels. By estimating conditional quantiles directly, prediction intervals can be constructed without assuming a specific distribution of prediction errors. Moreover, the quantile loss can be readily integrated into the existing neural network framework, enabling the point prediction model to be extended directly to interval prediction. Although alternative uncertainty estimation methods such as conformal prediction are also applicable, quantile regression is selected because of its direct compatibility with the prediction objective and the existing network structure. Then, the MAE loss in the BKA-CNN-LSTM prediction model was transformed into a quantile loss function $L$, which is expressed as

$$Q_{y_i}(\tau|\boldsymbol{x}_i) = \boldsymbol{\beta}(\tau)\boldsymbol{x}_i, i = 1, 2, \cdots, n \tag{5}$$

$$L = \sum_{i=1}^{n} \gamma_\tau [y_i - \boldsymbol{x}_i^{\mathrm{T}} \boldsymbol{\beta}(\tau)] \tag{6}$$

where $Q$ is the conditional quantile; $\beta$ is the vector of regression coefficients; $L$ is the loss function; and $\gamma_\tau$ is the absolute value function of the tilt.

For a confidence level of, the lower and upper bounds are defined by the and conditional quantiles. Therefore, the 95% prediction interval corresponds to the 0.025 and 0.975 quantiles, while the 85% interval corresponds to the 0.075 and 0.925 quantiles. The four quantile models are trained separately using the same BKA optimized CNN LSTM configuration, and BKA optimization is not repeated for different quantile levels.

To evaluate the accuracy level of parameter interval results inverted through different sets of measurement points, interval coverage probability (PICP), and prediction interval normalized average width (PINAW) are introduced to evaluate the reliability of the upper and lower limits of the interval for each settlement measurement point. Among them, PICP measures the empirical coverage probability of the prediction interval, and its proximity to the nominal coverage level reflects the calibration and reliability of the interval. PINAW measures the normalized average width of the prediction interval and primarily reflects interval sharpness. A smaller PINAW indicates a narrower and sharper prediction interval, but it does not necessarily imply better predictive performance unless adequate empirical coverage is simultaneously maintained. Therefore, PICP and PINAW should be interpreted jointly: a desirable prediction interval should maintain adequate coverage while remaining as narrow as possible. The calculation of the above indicators is as follows:

$$PICP = \frac{1}{n} \sum_{i=1}^{n} b_i \tag{7}$$

$$PINAW = \frac{1}{nR} \sum_{i=1}^{n} (U(\lambda_i) - L(\lambda_i)) \tag{8}$$

where $n$ is the number of prediction samples; $b_i$ is an indicator variable equal to 1 if the observed value $y_i$ lies within the prediction interval [$L_i$,$U_i$] and 0 otherwise; $L_i$ and $U_i$ denote the lower and upper bounds of the prediction interval for the $i$-th sample, respectively; and $R = y_{max} - y_{min}$ denotes the range of the observed target values.

Since PICP and PINAW characterize complementary aspects of prediction-interval quality and may exhibit a trade-off between coverage and interval width, the coverage width-based criterion (CWC) is further adopted to evaluate these two properties

jointly. In order to further evaluate the accuracy of the model more accurately, the coverage width-based criterion (CWC) is used to comprehensively evaluate the quality of interval prediction:

$$CWC = R \cdot PINAW \cdot \left(1 + \gamma(PICP)e^{-\eta(PICP-\mu)}\right) \tag{9}$$

where $R$ denotes the range of the observed target values; $\mu$ denotes the nominal coverage probability corresponding to the prescribed prediction interval, i.e., $\mu$ = 0.95 and 0.85 for the 95% and 85% prediction intervals, respectively; $\eta$ is a penalty parameter controlling the magnitude of the coverage penalty and is set to 30 in this study; and $\gamma$(PICP) is an indicator function defined as

$$\gamma(PICP) = \begin{cases} 0, PICP > \mu \\ 1, PICP < \mu \end{cases} \tag{10}$$

Thus, no additional coverage penalty is imposed when the empirical coverage reaches or exceeds the nominal level, whereas an exponential penalty is introduced when the empirical coverage falls below the nominal level.

Based on the BKA-CNN-LSTM model and combined with quantile regression model, establish a displacement interval prediction model for concrete dams. The specific steps are as follows.

Step 1: Preprocess the dam displacement data and environmental feature variables, and divide the processed data chronologically into a training set, a validation set, and an untouched final test set.

Step 2: Build a CNN-LSTM model, input the training set data, and use the BKA to optimize the hyperparameters of the model to determine the hyperparameters of the network model.

Step 3: Set the mean absolute error (MAE) as the fitness function and train the BKA-CNN-LSTM dam displacement prediction model.

Step 4: After the model configuration and hyperparameter selection are finalized, input the untouched final test set into the trained BKA-CNN-LSTM model and evaluate its predictive performance using the specified evaluation metrics.

Step 5: With the optimized CNN LSTM configuration fixed, train the QR models at quantile levels of 0.025, 0.075, 0.925, and 0.975, and construct the corresponding 95% and 85% prediction intervals for dam displacement.

In summary, the implementation process for the deformation interval prediction model for concrete dams is shown in Figure 4.

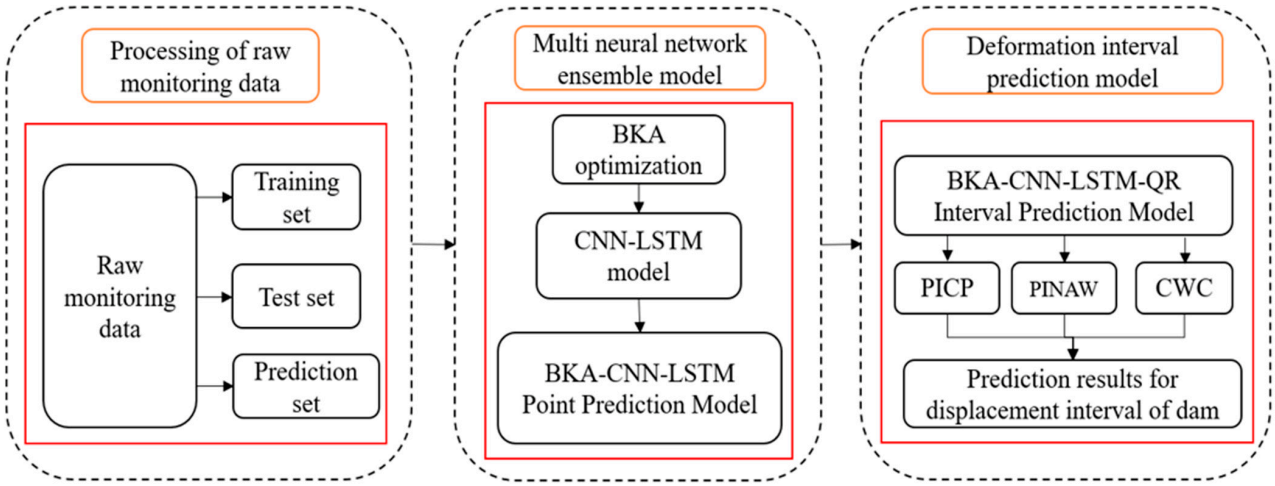



**Figure 4.** Flowchart of Interval Prediction Model Based on BKA-CNN-LSTM-QR.

## 4. Case Study

### *4.1. Project Overview*

The hydropower station considered in this study is primarily designed for power generation. The project is classified as a Grade II large-scale project, with the main hydraulic structures classified as Grade (2) structures. The retaining dam of the hydraulic complex is a concrete dam. To establish stable reference points for deformation monitoring, one inverted plumb system is arranged at each dam abutment, namely B1-IP-01 on the left bank and B15-IP-01 on the right bank. In addition, one plumb line and one inverted plumb line, denoted as B12-PL-01 and B12-IP-01, respectively, are installed in the powerhouse dam section and in the observation room of the foundation gallery. The working principles of the plumb line systems are illustrated in Figure 5, where Figure 5a shows the layout of the inverted plumb line and Figure 5b presents the layout of the plumb line.

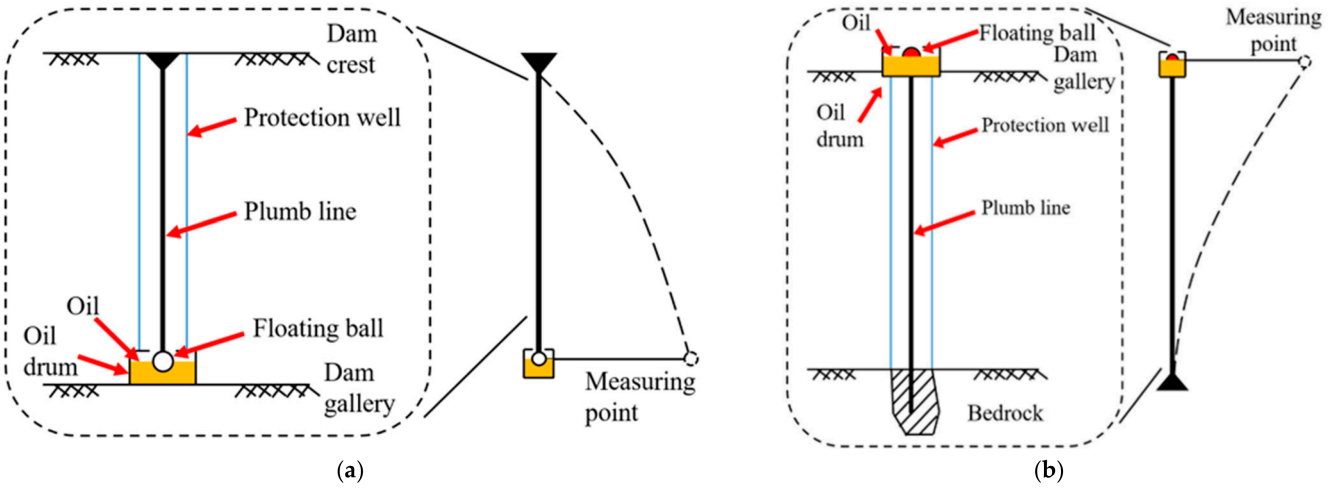



**Figure 5.** Working principle diagram of the plumb line. (**a**) Inverted plumb line layout diagram; (**b**) plumb line layout diagram.

In this study, the monitoring data obtained from the plumb line and inverted plumb line associated with measuring point B12-IP-01 in the 12th dam section were selected as the research object for constructing the deformation prediction model. Missing observations in the monitoring series were supplemented using linear interpolation between adjacent valid observations, resulting in a total of 1226 valid data points. To facilitate model training and prediction, the temporal variation process of the monitoring data is presented in Figure 6. The dataset was divided chronologically into three mutually exclusive subsets: 982 samples for model training, 122 subsequent samples for validation and hyperparameter selection, and the remaining 122 samples as an untouched final test set. The validation set was used only for hyperparameter optimization and model selection, whereas the final test set was not involved in model training, hyperparameter optimization, or model selection and was used only for the final out-of-sample performance evaluation.

### *4.2. Model Parameter Setting and Optimization*

During the operation of dams, they are subject to complex environmental factors, among which the deformation of concrete dams is mainly affected by water pressure factors, temperature factors, and aging factors. In order to simulate these factors in the model, this paper determines the eigenvalues of the predictive model. Among them, the water pressure factor adopts $H$, $H^2$, $H^3$, and $H^4$, the temperature factor adopts harmonic factor $\sin\frac{2\pi it}{365}$ and $\cos\frac{2\pi it}{365}$ to simulate temperature changes, and the aging factor adopts $\ln\theta$.

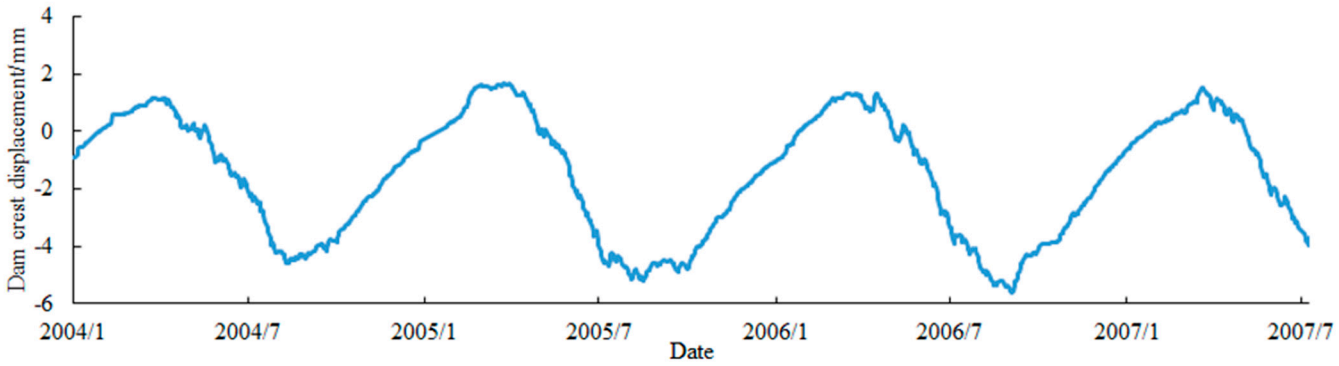



**Figure 6.** The process line of the monitoring data for dam crest displacement.

In the BKA-based optimization procedure, six hyperparameters of the CNN LSTM model are optimized simultaneously, including the number of CNN filters, convolution kernel size, CNN activation function, number of LSTM units, time step, and learning rate. Their search spaces are {8, 16, 32, 64}, {3, 5, 7}, {ReLU, tanh, sigmoid, softmax}, {64, 128, 256}, {5, 10}, and {0.001, 0.01}, respectively. The MAE on the validation set is used as the fitness function to evaluate each candidate parameter combination. Other parameters, including padding, stride, pooling size, dropout rate, optimizer, batch size, and training epochs, are kept fixed during optimization. All the parameter settings are shown in Table 1.

**Table 1.** The BKA-CNN-LSTM parameter settings.

| Parameter | | Take a Value |
|---|---|---|
| Convolutional Layer | filters | 64 |
| | Kernel_size | 5 |
| | padding | same |
| | strides | 1 |
| | activation | tanh |
| Pooling layer | pool_size | 1 |
| LSTM layer | units | 256 |
| | Time step | 10 |
| | activation | tanh |
| | optimizer | Adam; the learning rate is 0.01 |
| | batch_size | 64 |
| | epochs | 500 |

(1) In the convolutional layer, the number of convolution kernels and filters can be selected between 8, 16, 32, and 64. The kernel size should be selected between 3, 5, and 7. In convolutional neural networks, 'padding' is used to control the edge processing of input data during convolution operations. Choosing 'same' means zero padding is applied to the edges of the input data to maintain the output size consistent with the input. The stride of the convolutional kernel on the input data is set to a default value of 1 to preserve more information. Comparison of activation functions between 'relu', 'tanh', 'sigmoid' and 'softmax'.

(2) In the pooling layer, select pool_2 as 1, do not perform pooling, and maintain the original feature map size.

(3) In the LSTM layer, the number of neurons units in the fully connected layer is selected between 64, 128, and 256. Choose a time step between 5 and 10. Choose Adam as the optimizer and debug with a learning rate between 0.01 and 0.001. Select the same convolutional layer for the remaining parameters. In addition, to suppress the overfitting

phenomenon of LSTM, a dropout layer needs to be added, and dropout is debugged between them, with a final setting of 0.2. Specify the loss function 'mean_Squared_error' and optimizer type 'adam' to verify that the data does not participate in training.

For a fair comparison, BKA, DBO, and POA were implemented using the same computational settings, including the population size, maximum number of iterations, CNN LSTM hyperparameter search space, validation dataset, fitness function, and initialization strategy. Specifically, the population size and maximum number of iterations were set to 30 and 200, respectively, and the MAE calculated on the validation set was adopted as the fitness function. The initial populations were randomly generated within the prescribed search ranges. The optimization process was terminated when the maximum number of 200 iterations was reached, corresponding to a maximum fitness evaluation budget of 6000 for each algorithm. Therefore, the three algorithms differed only in their population update mechanisms and algorithm specific control parameters.

### *4.3. Model Point Prediction Results and Analysis*

To comprehensively evaluate the predictive performance of the BKA-CNN-LSTM model, several benchmark models were constructed, including CNN, LSTM, GRU, Transformer, DBO-CNN-LSTM optimized by the beetle optimization algorithm, and POA-CNN-LSTM optimized by the pelican optimization algorithm. To evaluate the influence of random initialization, the proposed model is independently trained five times using different random seeds while keeping the data partition and model parameters unchanged. The mean values and standard deviations of the main evaluation metrics are reported to assess the stability of the model.

The processed monitoring data and corresponding environmental features of measuring point B12-IP-01 were input into each model under the same data partition and training conditions. The fitting performance of the training set is summarized in Table 2. The present study focuses on a single monitoring point of one concrete dam. Therefore, the current case study mainly verifies the feasibility of the proposed framework, while its applicability to other monitoring locations and dams requires further validation. As shown in Table 2, all models achieved satisfactory fitting accuracy, indicating that the selected network structures were reasonably configured and could therefore be used for subsequent comparative evaluation on the final test set in the present case study.

**Table 2.** Training set fitting accuracy.

| Algorithm | MAE/mm | MAPE/% | MSE/mm$^2$ | RMSE/mm | $R^2$ |
|---|---|---|---|---|---|
| BKA-CNN-LSTM | 0.1065 | 0.1643 | 0.0209 | 0.1444 | 0.9956 |
| CNN | 0.2031 | 0.1743 | 0.0718 | 0.2679 | 0.9849 |
| LSTM | 0.2382 | 0.2218 | 0.1011 | 0.3179 | 0.9787 |
| Transformer | 0.2405 | 0.2125 | 0.1128 | 0.3358 | 0.9713 |
| GRU | 0.2225 | 0.2436 | 0.0981 | 0.3132 | 0.9821 |
| DBO-CNN-LSTM | 0.2041 | 0.4278 | 0.0722 | 0.2688 | 0.9848 |
| POA-CNN-LSTM | 0.2864 | 0.3637 | 0.1392 | 0.3731 | 0.9706 |

Input the prediction set data into the trained models for prediction. The comparison between the prediction curves of each model and the true values is shown in Figure 7. From Figure 7, it can be seen that, compared to other prediction models, the displacement predicted by the BKA-CNN-LSTM model is closest in magnitude to the measured values and most consistent in trend with the measured values, indicating that the model has strong learning and prediction abilities.

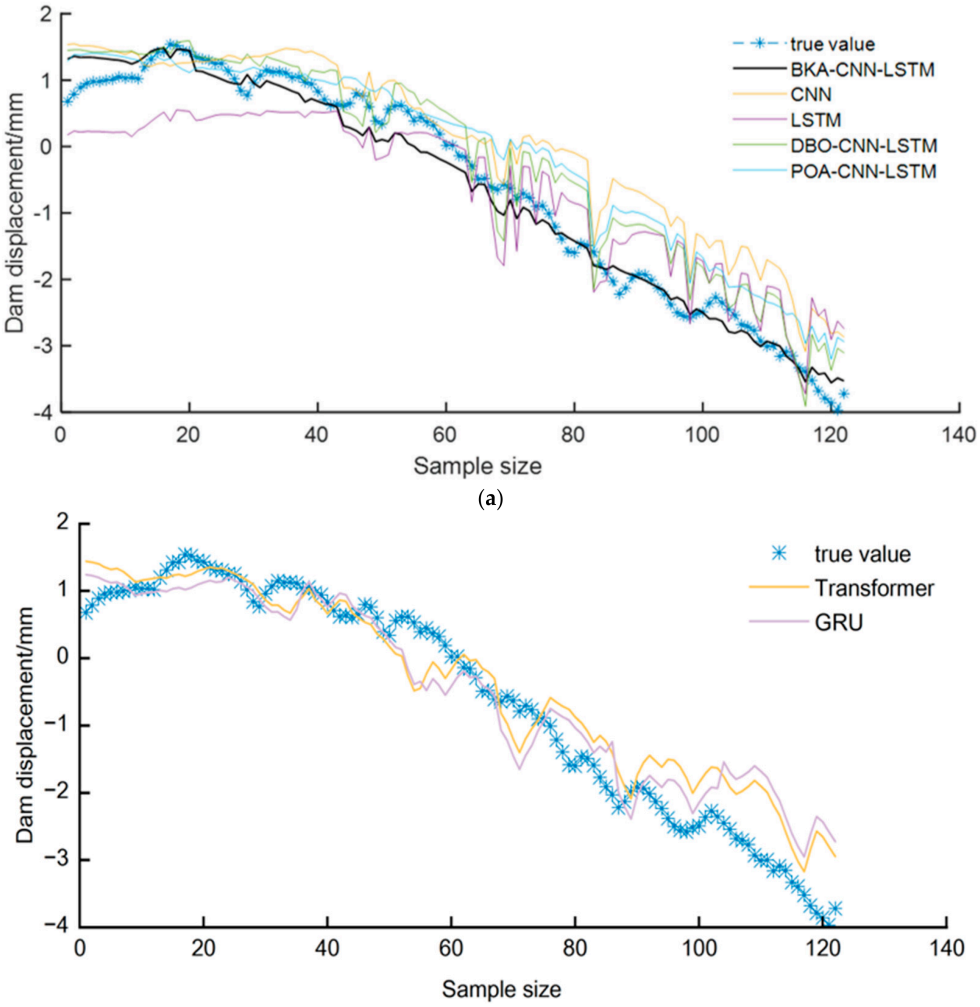



**Figure 7.** Comparison of point prediction results on the final test set. (**a**) Measured displacement and prediction results obtained by the BKA-CNN-LSTM, CNN, LSTM, DBO-CNN-LSTM, and POA-CNN-LSTM models; (**b**) measured displacement and prediction results obtained by the Transformer and GRU modelsl.

To further evaluate the predictive performance of each model, multiple evaluation metrics, including *MAE*, *MAPE*, *MSE*, *RMSE*, $R^2$, and computation time, were used to quantify the predictive performance of the models. The evaluation metrics for the model prediction set are shown in Table 3.

**Table 3.** Model point prediction results.

| Algorithm | *MAE*/mm | *MAPE*/% | *MSE*/mm$^2$ | *RMSE*/mm | $R^2$ | Time/t |
|---|---|---|---|---|---|---|
| BKA-CNN-LSTM | 0.2188 ± 0.0067 | 0.5121 ± 0.0184 | 0.0690 ± 0.0041 | 0.2627 ± 0.0078 | 0.9749 ± 0.0021 | 80.96 ± 1.84 |
| CNN | 0.6503 ± 0.0215 | 0.6748 ± 0.0269 | 0.6243 ± 0.0328 | 0.7901 ± 0.0207 | 0.7732 ± 0.0116 | 68.04 ± 1.21 |
| LSTM | 0.5894 ± 0.0187 | 0.5516 ± 0.0223 | 0.4449 ± 0.0264 | 0.6670 ± 0.0198 | 0.8384 ± 0.0095 | 73.74 ± 1.58 |
| Transformer | 0.4295 ± 0.0146 | 0.3216 ± 0.0152 | 0.2793 ± 0.0184 | 0.5285 ± 0.0173 | 0.9242 ± 0.0068 | 64.35 ± 1.42 |
| GRU | 0.4316 ± 0.0168 | 0.4876 ± 0.0195 | 0.3144 ± 0.0201 | 0.5608 ± 0.0181 | 0.9188 ± 0.0074 | 75.21 ± 1.63 |
| DBO-CNN-LSTM | 0.4460 ± 0.0205 | 0.8223 ± 0.0367 | 0.2821 ± 0.0247 | 0.5311 ± 0.0226 | 0.8975 ± 0.0098 | 169.54 ± 4.91 |
| POA-CNN-LSTM | 0.4933 ± 0.0238 | 0.7269 ± 0.0314 | 0.3612 ± 0.0295 | 0.6010 ± 0.0249 | 0.8688 ± 0.0113 | 189.23 ± 5.36 |

According to Table 3, the BKA-CNN-LSTM model achieved mean MAE, MSE, and RMSE values of 0.2188 mm, 0.0690 mm$^2$, and 0.2627 mm, respectively, all of which were the lowest among the compared models. It also obtained the highest $R^2$ value of 0.9749, indicating that its predictions were closest to the measured values and that it provided the

best overall fitting performance. Compared with the CNN, LSTM, Transformer, GRU, DBO-CNN-LSTM, and POA-CNN-LSTM models, the MAE of BKA-CNN-LSTM was reduced by 66.35%, 62.88%, 49.06%, 49.30%, 50.94%, and 55.65%, respectively, while its RMSE was reduced by 66.75%, 60.61%, 50.29%, 53.16%, 50.54%, and 56.29%, respectively. In addition, its $R^2$ increased by 26.09%, 16.28%, 5.49%, 6.11%, 8.62%, and 12.21%, respectively. These results demonstrate that the BKA-based optimization of the CNN-LSTM network can effectively reduce the overall prediction error and improve the model's ability to capture the variation characteristics of dam displacement.

It should be noted that the Transformer model achieved the lowest MAPE of 0.3216%, outperforming the BKA-CNN-LSTM model, whose MAPE was 0.5121%. The GRU model also obtained a slightly lower MAPE of 0.4876%. Therefore, BKA-CNN-LSTM did not achieve the best result for every individual metric. Nevertheless, it showed the best performance in terms of MAE, MSE, RMSE, and $R^2$, demonstrating superior overall prediction performance.

Regarding computational efficiency, the Transformer model required the shortest running time of 64.35 s, followed by CNN and LSTM at 68.04 s and 73.74 s, respectively. The running time of BKA-CNN-LSTM was 80.96 s, which was slightly longer than those of the single deep-learning models but substantially shorter than the 169.54 s required by DBO-CNN-LSTM and the 189.23 s required by POA-CNN-LSTM, corresponding to reductions of approximately 52.25% and 57.21%, respectively. This indicates that the BKA-CNN-LSTM model maintains relatively high optimization efficiency while considerably improving prediction accuracy. The iterative convergence processes of BKA, DBO, and POA are presented in Figure 8.

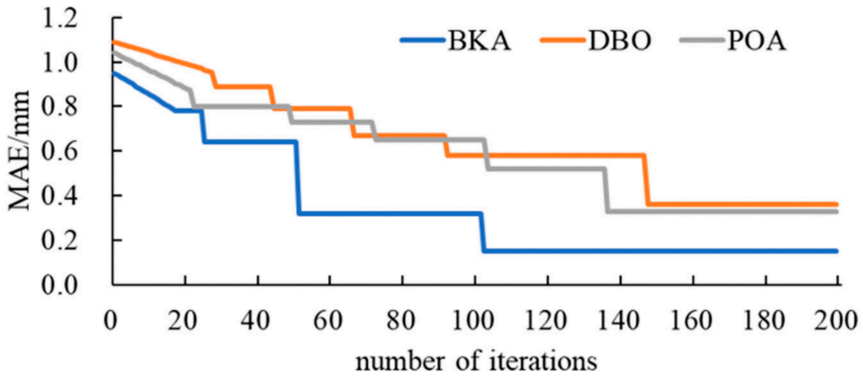



**Figure 8.** The number of iterations for each optimization algorithm.

To quantitatively evaluate the contributions of CNN, LSTM, and BKA to dam displacement point prediction, five ablation models were constructed, namely CNN, LSTM, CNN-BKA, LSTM-BKA, and BKA-CNN-LSTM. Their performance was evaluated using MAE, MAPE, MSE, RMSE, and $R^2$. As shown in Table 4, the individual CNN and LSTM models exhibited relatively large prediction errors. The CNN model yielded an MAE of 0.6503 mm and an RMSE of 0.7901 mm, whereas the corresponding values of the LSTM model were 0.5894 mm and 0.6670 mm. Compared with CNN, LSTM achieved lower prediction errors and a higher $R^2$, indicating that LSTM can better capture temporal dependencies in the dam displacement sequence.

After introducing BKA optimization, the predictive performance of both CNN-BKA and LSTM-BKA was improved. For CNN-BKA, the MAE, MSE, and RMSE decreased to 0.4234 mm, 0.3276 $mm^2$, and 0.5724 mm, respectively, while $R^2$ increased to 0.8765. The corresponding values for LSTM-BKA were further improved to 0.3827 mm, 0.2564 $mm^2$, 0.5064 mm, and 0.9012. These results demonstrate that BKA can effectively

reduce prediction errors and enhance fitting performance by optimizing the key model parameters. Moreover, LSTM-BKA outperformed CNN-BKA, further confirming the importance of temporal dependency learning in dam displacement prediction.

**Table 4.** Ablation Results of the BKA-CNN-LSTM Point Prediction Model.

| BKA-CNN-LSTM | | | *MAE*/mm | *MAPE*/% | *MSE*/mm$^2$ | *RMSE*/mm | $R^2$ |
|---|---|---|---|---|---|---|---|
| CNN | LSTM | BKA | | | | | |
| √ | | | 0.6503 | 0.6748 | 0.6243 | 0.7901 | 0.7732 |
| | √ | | 0.5894 | 0.5516 | 0.4449 | 0.6670 | 0.8384 |
| √ | | √ | 0.4234 | 0.5432 | 0.3276 | 0.5724 | 0.8765 |
| | √ | √ | 0.3827 | 0.5264 | 0.2564 | 0.5064 | 0.9012 |
| √ | √ | √ | **0.2188** | **0.5121** | **0.0690** | **0.2627** | **0.9749** |

Checkmark indicates the method used in single-round model, while bold metrics shows the best of all results.

The complete BKA-CNN-LSTM model achieved the best overall performance, with MAE, MAPE, MSE, and RMSE values of 0.2188 mm, 0.5121%, 0.0690 mm$^2$, and 0.2627 mm, respectively, and an $R^2$ of 0.9749. Compared with CNN and LSTM, its MAE was reduced by 66.35% and 62.88%, respectively, while its RMSE was reduced by 66.75% and 60.61%. Its $R^2$ increased by 26.09% and 16.28%, respectively. Compared with CNN-BKA and LSTM-BKA, the RMSE of the complete model was further reduced by 54.11% and 48.12%, respectively. These findings indicate that the local feature extraction ability of CNN, the temporal dependency learning capability of LSTM, and the parameter optimization ability of BKA are complementary. Their integration substantially improves the extraction of nonlinear displacement characteristics and leads to higher point prediction accuracy.

### *4.4. Model Interval Prediction Results and Analysis*

Based on the optimized BKA CNN LSTM model, the 95% prediction interval is constructed from the 0.025 and 0.975 conditional quantiles, while the 85% prediction interval is constructed from the 0.075 and 0.925 conditional quantiles. The corresponding interval prediction results are shown in Figure 9.

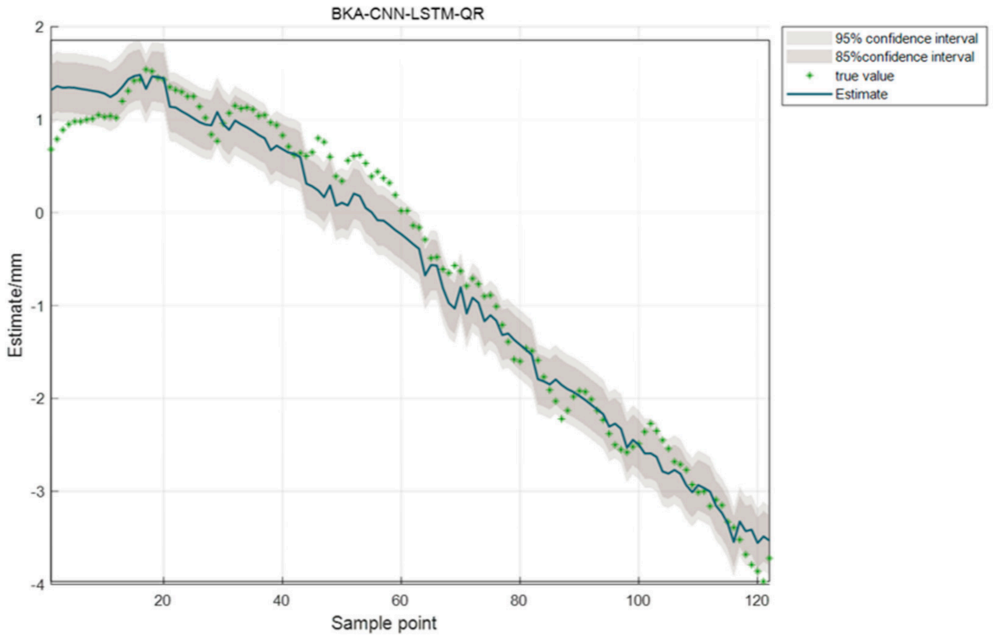



**Figure 9.** Interval prediction of BKA-CNN-LSTM-QR model.

As shown in Figure 9, the prediction intervals generally follow the variation trend of the measured displacement and provide good coverage of the observed values. The 95% interval provides a higher coverage rate, whereas a few local deviations can be observed in the narrower 85% interval. These deviations are mainly associated with short-term fluctuations in the displacement sequence, which may not be fully represented by the historical samples used for model training. Overall, the proposed model maintains good interval coverage while preserving a relatively narrow prediction range, indicating a reasonable balance between reliability and sharpness.

To verify the performance of the BKA-CNN-LSTM-QR model in interval prediction, models were constructed for interval prediction and comparison. The interval prediction evaluation indicators of each model at 95% and 85% confidence levels are shown in Table 5 and Figure 10.

**Table 5.** Different model interval prediction error.

| Model | PICP | | PINAW | | CWC | |
|---|---|---|---|---|---|---|
| | 95% | 85% | 95% | 85% | 95% | 85% |
| BKA-CNN-LSTM-QR | **0.9918** | **0.8525** | **0.1349** | **0.0991** | **0.2848** | **0.2145** |
| CNN-QR | 0.9344 | 0.4098 | 0.4723 | 0.1433 | 0.9521 | 0.3659 |
| LSTM-QR | 0.8894 | 0.7894 | 0.3601 | 0.2263 | 0.3637 | 0.4635 |
| Transformer-QR | 0.8921 | 0.6527 | 0.3925 | 0.2678 | 0.5148 | 0.4512 |
| GRU-QR | 0.9215 | 0.7214 | 0.4273 | 0.3721 | 0.4527 | 0.3615 |
| DBO-CNN-LSTM-QR | 0.7213 | 0.5738 | 0.1961 | 0.1531 | 0.4425 | 0.3549 |
| POA-CNN-LSTM-QR | 0.8525 | 0.6639 | 0.2514 | 0.1783 | 0.5286 | 0.3930 |

Bold numbers indicates the best-performing results among the many.

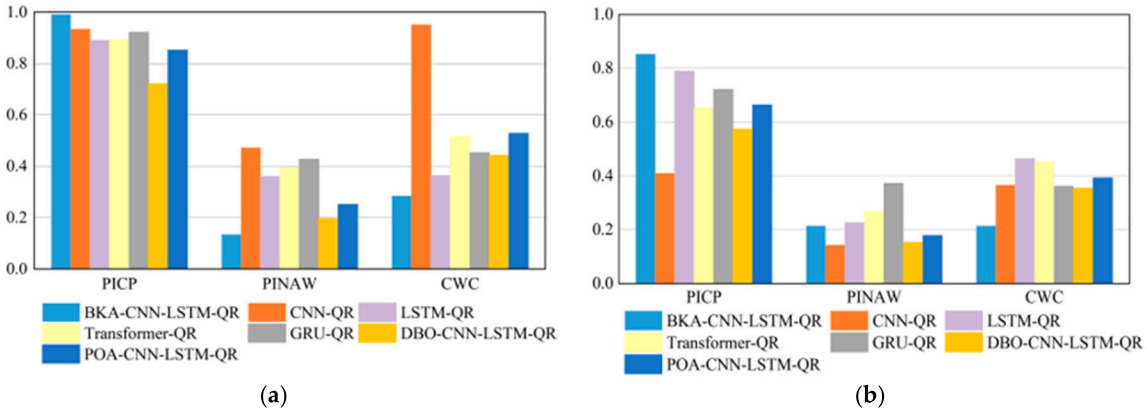



**Figure 10.** Different model interval prediction error. (**a**) 95% confidence level; (**b**) 85% confidence level.

A comprehensive comparison of Table 5 and Figure 10 shows that the BKA-CNN-LSTM-QR model achieved superior interval prediction performance at both the 95% and 85% confidence levels. At the 95% confidence level, the proposed model obtained a PICP of 0.9918, which was higher than the values of 0.7213–0.9344 achieved by the other models. Its coverage probability was therefore improved by 6.14–37.50%, indicating that the prediction interval covered a larger proportion of the measured displacement values. It should be noted that the PICP of 0.9918 was slightly higher than the nominal confidence level of 0.95, suggesting strong interval coverage but also a certain degree of conservativeness. At the 85% confidence level, the PICP was 0.8525, which was very close to the nominal value of 0.85, demonstrating favorable reliability and calibration of the prediction interval.

In terms of interval width, the PINAW values of the BKA-CNN-LSTM-QR model were 0.1349 and 0.0991 at the 95% and 85% confidence levels, respectively, both of which were the lowest among all the compared models. At the 95% confidence level, the PINAW was

reduced by 31.21–71.44% relative to the other models, while at the 85% confidence level, it was reduced by 30.84–73.37%. These results indicate that the proposed model can generate more compact prediction intervals while maintaining a high coverage probability, thereby improving the sharpness and effectiveness of interval prediction.

Moreover, the CWC values of the proposed model were 0.2848 and 0.2145 at the 95% and 85% confidence levels, respectively, which were also the lowest among all models. At the 95% confidence level, the CWC was reduced by 21.69–70.09% compared with the competing models, while at the 85% confidence level, the reduction ranged from 39.56% to 53.72%. Overall, the BKA-CNN-LSTM-QR model achieved a better balance between interval coverage and interval width. It not only provided sufficient coverage of the measured displacement values but also avoided excessively wide prediction intervals, demonstrating reliable interval forecasting performance and effective quantification of the conditional predictive uncertainty of dam displacement.

To further investigate the contributions of CNN, LSTM, and BKA to interval prediction, five interval forecasting models were constructed: CNN-QR, LSTM-QR, CNN-BKA-QR, LSTM-BKA-QR, and BKA-CNN-LSTM-QR. Their performance was evaluated using PICP, PINAW, and CWC. As shown in Table 6, CNN-QR and LSTM-QR suffered from either insufficient coverage or excessively wide prediction intervals. For example, at the 85% confidence level, the PICP of CNN-QR was only 0.4098, which was substantially lower than the nominal coverage level of 0.85. Although the PICP of LSTM-QR increased to 0.7894, its PINAW reached 0.2263, indicating a relatively wide prediction interval.

**Table 6.** Ablation Results of the BKA-CNN-LSTM-QR Interval Prediction Model.

| BKA-CNN-LSTM-QR | | | PICP (95%) | PICP (85%) | PINAW (95%) | PINAW (85%) | CWC (95%) | CWC (85%) |
|---|---|---|---|---|---|---|---|---|
| CNN | LSTM | BKA | | | | | | |
| √ | | | 0.9344 | 0.4098 | 0.4723 | 0.1433 | 0.9521 | 0.3659 |
| | √ | | 0.8894 | 0.7894 | 0.3601 | 0.2263 | 0.3637 | 0.4635 |
| √ | | √ | 0.9425 | 0.6421 | 0.2948 | 0.1284 | 0.7612 | 0.2975 |
| | √ | √ | 0.9027 | 0.8276 | 0.2472 | 0.1648 | 0.3481 | 0.3617 |
| √ | √ | √ | **0.9918** | **0.8525** | **0.1349** | **0.0991** | **0.2848** | **0.2145** |

Checkmark indicates the method used in single-round model, while bold metrics shows the best of all results.

After BKA optimization was introduced, the interval prediction quality of CNN-BKA-QR and LSTM-BKA-QR was generally improved. At the 95% confidence level, the PICP of CNN-BKA-QR increased to 0.9425, while its PINAW decreased from 0.4723 for CNN-QR to 0.2948. The PICP of LSTM-BKA-QR was 0.9027, and its PINAW decreased from 0.3601 for LSTM-QR to 0.2472. The corresponding CWC values were also substantially reduced, indicating that BKA improved not only interval coverage but also interval sharpness, thereby enhancing the overall quality of interval prediction.

The complete BKA-CNN-LSTM-QR model achieved the best results at both confidence levels. Its PICP values were 0.9918 and 0.8525 at the 95% and 85% confidence levels, respectively. In particular, the empirical coverage of 0.8525 was very close to the nominal level of 0.85, demonstrating favorable interval calibration. Meanwhile, its PINAW values were 0.1349 and 0.0991, both of which were the lowest among the ablation models. Its CWC values of 0.2848 and 0.2145 were also the lowest. Compared with CNN-QR, the complete model reduced PINAW by 71.44% and 30.84% at the 95% and 85% confidence levels, respectively, and reduced CWC by 70.09% and 41.38%. Compared with LSTM-QR, PINAW was reduced by 62.54% and 56.21%, while CWC was reduced by 21.69% and 53.72%. The complete model also achieved higher coverage and smaller interval widths than CNN-BKA-QR and LSTM-BKA-QR.

Overall, CNN, LSTM, and BKA all contributed positively to interval prediction. CNN extracts local correlations among environmental variables, LSTM captures long-term temporal dependencies in dam displacement, and BKA improves the stability and accuracy of quantile predictions through parameter optimization. Their integration enables BKA-CNN-LSTM-QR to increase interval coverage while effectively narrowing the prediction interval, thereby achieving a better balance between reliability and sharpness.

## 5. Conclusions

(1) To address the limitations of conventional point prediction models in comprehensively characterizing the fluctuations and predictive uncertainty of dam displacement, this study integrates the local feature extraction capability of CNN with the temporal dependency learning capability of LSTM and employs BKA to optimize the key hyperparameters of the CNN-LSTM model, thereby constructing a BKA-CNN-LSTM point prediction model. Its overall performance in dam displacement prediction is evaluated through comparisons with CNN, LSTM, GRU, Transformer, DBO-CNN-LSTM, and POA-CNN-LSTM. On this basis, quantile regression is further incorporated to develop the BKA-CNN-LSTM-QR interval prediction model, enabling the simultaneous characterization of dam displacement trends and their associated conditional predictive uncertainty.

(2) The comparative results show that BKA effectively improves the hyperparameter optimization of the CNN LSTM model. The proposed BKA CNN LSTM model achieves the best performance in terms of MAE, MSE, and RMSE, although Transformer and GRU obtain slightly lower MAPE values. Overall, the proposed model demonstrates favorable prediction accuracy and fitting performance for the investigated dam displacement data.

(3) The prediction results of the BKA-CNN-LSTM-QR interval prediction model are more stable and reliable compared to other models, and the interval evaluation indicators are superior to other prediction models. For the investigated dam and monitoring point, the proposed interval prediction model effectively characterizes the conditional predictive uncertainty of displacement and provides prediction intervals as a useful supplement to deterministic point predictions. These results demonstrate the feasibility of the proposed framework for the present case.

(4) The present model is established for the temporal prediction of deformation at a single monitoring point, and spatial relationships among multiple monitoring locations are not considered. In future studies, monitoring data from multiple measuring points can be incorporated to investigate the spatial correlation of dam deformation and to extend the current framework to multivariate spatial and temporal deformation prediction. In addition, abrupt deformation changes and extreme operating conditions that are insufficiently represented in the training data may lead to local prediction interval failures.

**Author Contributions:** Conceptualization, F.H. and C.G.; methodology, F.H.; software, F.H.; validation, P.L. and X.C.; formal analysis, F.H.; investigation, F.H. and P.L.; resources, C.G.; data curation, P.L. and X.C.; writing—original draft preparation, F.H.; writing—review and editing, C.G., P.L. and X.C.; visualization, X.C.; supervision, C.G.; project administration, C.G.; funding acquisition, C.G. All authors have read and agreed to the published version of the manuscript.

**Funding:** This research was supported by the National Natural Science Foundation of China (No. 52579119, 52379122) and the National Key Research and Development Program of China (No. 2024YFC3210700).

**Institutional Review Board Statement:** The authors choose to exclude this statement because the study did not require ethical approval.

**Informed Consent Statement:** The authors choose to exclude this statement because the study did not involve humans.

**Data Availability Statement:** All relevant data are within the manuscript.

**Acknowledgments:** The authors are grateful to National Natural Science Foundation of China and the National Key Research and Development Program of China for providing the necessary funding to conduct this research.

**Conflicts of Interest:** The authors declare no conflicts of interest.

## Abbreviations

The following abbreviations are used in this manuscript:

| | |
|---|---|
| BKA | Black winged Kite Optimization Algorithm |
| CNN | Convolutional Neural Network |
| LSTM | Long Short Term Memory |
| QR | Quantile regression |

## References

1. Widiasari, I.R.; Efendi, R. Utilizing LSTM-GRU for IOT-Based Water Level Prediction Using Multi-Variable Rainfall Time Series Data. *Informatics* **2024**, *11*, 73. [CrossRef]
2. Mata, J. Interpretation of concrete dam behaviour with artificial neural network and multiple linear regression models. *Eng. Struct.* **2011**, *33*, 903–910. [CrossRef]
3. Frau, L.; Susto, G.A.; Barbariol, T.; Feltresi, E. Uncertainty Estimation for Machine Learning Models in Multiphase Flow Applications. *Informatics* **2021**, *8*, 58. [CrossRef]
4. Salazar, F.; Morán, R.; Toledo, M.Á.; Oñate, E. Data-Based Models for the Prediction of Dam Behaviour: A Review and Some Methodological Considerations. *Arch. Comput. Methods Eng.* **2017**, *24*, 1–21. [CrossRef]
5. Brownjohn, J.M.W. Structural health monitoring of civil infrastructure. *Philos. Trans. A Math. Phys. Eng. Sci.* **2007**, *365*, 589–622. [CrossRef] [PubMed]
6. Tao, L.; Zheng, D.; Wu, X.; Chen, X.; Liu, Y.; Chen, Z.; Jiang, H. Stress Estimation of Concrete Dams in Service Based on Deformation Data Using SIE–APSO–CNN–LSTM. *Water* **2023**, *15*, 59. [CrossRef]
7. Kang, F.; Liu, X.; Li, J. Temperature effect modeling in structural health monitoring of concrete dams using kernel extreme learning machines. *Struct. Health Monit.* **2020**, *19*, 987–1002. [CrossRef]
8. Li, M.; Pan, J.; Liu, Y.; Wang, Y.; Zhang, W.; Wang, J. Dam Deformation Forecasting Using SVM-DEGWO Algorithm Based on Phase Space Reconstruction. *PLoS ONE* **2022**, *17*, e0267434. [CrossRef] [PubMed]
9. Ranković, V.; Grujović, N.; Divac, D.; Milivojević, N. Development of Support Vector Regression Identification Model for Prediction of Dam Structural Behaviour. *Struct. Saf.* **2014**, *48*, 33–39. [CrossRef]
10. Gu, H.; Yang, M.; Gu, C.; Huang, X. A factor mining model with optimized random forest for concrete dam deformation monitoring. *Water Sci. Eng.* **2021**, *14*, 330–336. [CrossRef]
11. Léger, P.; Leclerc, M. Hydrostatic, Temperature, Time-Displacement Model for Concrete Dams. *J. Eng. Mech.* **2007**, *133*, 267–277. [CrossRef]
12. Wang, S.; Xu, Y.; Gu, C.; Bao, T.; Xia, Q.; Hu, K. Hysteretic Effect Considered Monitoring Model for Interpreting Abnormal Deformation Behavior of Arch Dams: A Case Study. *Struct. Control Health Monit.* **2019**, *26*, e2417. [CrossRef]
13. Wei, B.; Yuan, D.; Li, H.; Xu, Z. Combination forecast model for concrete dam displacement considering residual correction. *Struct. Health Monit.* **2019**, *18*, 232–244. [CrossRef]
14. Bui, K.T.T.; Tien Bui, D.; Zou, J.; Doan, C.; Revhaug, I. A novel hybrid artificial intelligent approach based on neural fuzzy inference model and particle swarm optimization for horizontal displacement modeling of hydropower dam. *Neural Comput. Appl.* **2018**, *29*, 1495–1506. [CrossRef]
15. Kang, F.; Liu, J.; Li, J.; Li, S. Concrete Dam Deformation Prediction Model for Health Monitoring Based on Extreme Learning Machine. *Struct. Control Health Monit.* **2017**, *24*, e1997. [CrossRef]
16. Su, H.; Li, X.; Yang, B.; Wen, Z. Wavelet Support Vector Machine-Based Prediction Model of Dam Deformation. *Mech. Syst. Signal Process.* **2018**, *110*, 412–427. [CrossRef]
17. Li, T.X.; Wang, F.; Liu, G.R. Dam deformation prediction method based on HHO-QRNN model. *Hydroelectr. Energy Sci.* **2024**, *42*, 117–120+116.
18. Zhang, M.; Chen, B.; Liu, W.; Qi, Y.; Zhang, M. Dam Deformation Prediction Model Selected by SSA-XGBoost. *Water Resour. Hydropower Eng.* **2024**, *55*, 142–153.
19. Lu, X.; Zhang, Y.; Wang, J.; Chen, Z. Dam Settlement Prediction Model Based on EMD-MGWO-LSTM. *Sci. Technol. Eng.* **2024**, *24*, 3268–3276.

20. Zhang, S.; Chen, Y.; Gu, C.; Yang, M. Deformation Prediction System of Concrete Dam Based on the IVM and RF Algorithm Optimized by SCSO. *Water* **2022**, *14*, 3739. [CrossRef]
21. Su, H.; Wen, Z.; Chen, Z.; Tian, S. Dam Safety Prediction Model Considering Chaotic Characteristics in Prototype Monitoring Data Series. *Struct. Health Monit.* **2016**, *15*, 639–649. [CrossRef]
22. Hüllermeier, E.; Waegeman, W. Aleatoric and epistemic uncertainty in machine learning: An introduction to concepts and methods. *Mach. Learn.* **2021**, *110*, 457–506. [CrossRef]
23. He, Y.; Liu, R.; Li, H.; Wang, S.; Lu, X. Short-term power load probability density forecasting method using kernel-based support vector quantile regression and Copula theory. *Appl. Energy* **2017**, *185*, 254–266. [CrossRef]
24. Zhang, C.; Zhao, Y.; Fan, C.; Li, T.; Zhang, X.; Li, J. A generic prediction interval estimation method for quantifying the uncertainties in ultra-short-term building cooling load prediction. *Appl. Therm. Eng.* **2020**, *173*, 115261. [CrossRef]
25. Zhu, X.; Zeng, B.; Dong, H.; Liu, J. An interval-prediction based robust optimization approach for energy-hub operation scheduling considering flexible ramping products. *Energy* **2020**, *194*, 116821. [CrossRef]
26. Hu, J.; Lin, Y.; Tang, J.; Zhao, J. A new wind power interval prediction approach based on reservoir computing and a quality-driven loss function. *Appl. Soft Comput.* **2020**, *92*, 106327. [CrossRef]
27. Wang, J.; Wang, W.; Hu, X. Black-winged kite algorithm: A nature-inspired meta-heuristic for solving benchmark functions and engineering problems. *Artif. Intell. Rev.* **2024**, *57*, 1–53. [CrossRef]
28. Choi, E.; Schuetz, A.; Stewart, W.F.; Sun, J. Using recurrent neural network models for early detection of heart failure onset. *J. Am. Med. Inform. Assoc.* **2017**, *24*, 361–370. [CrossRef] [PubMed]
29. Kong, W.; Dong, Z.Y.; Jia, Y.; Hill, D.J.; Xu, Y.; Zhang, Y. Short-Term Residential Load Forecasting Based on LSTM Recurrent Neural Network. *IEEE Trans. Smart Grid* **2017**, *10*, 841–851. [CrossRef]
30. Hanson, J.; Yang, Y.; Paliwal, K.; Zhou, Y. Improving protein disorder prediction by deep bidirectional long short-term memory recurrent neural networks. *Bioinformatics* **2017**, *33*, 685–692. [CrossRef] [PubMed]
31. Ozcanli, A.K.; Baysal, M. Islanding detection in microgrid using deep learning based on 1D CNN and CNN-LSTM networks. *Sustain. Energy Grids Netw.* **2022**, *32*, 100839. [CrossRef]
32. Jiang, Y.; Zhao, K.; Xia, K.; Xue, J.; Zhou, L.; Ding, Y.; Qian, P. A Novel Distributed Multitask Fuzzy Clustering Algorithm for Automatic MR Brain Image Segmentation. *J. Med. Syst.* **2019**, *43*, 118. [CrossRef] [PubMed]


**Disclaimer/Publisher's Note:** The statements, opinions and data contained in all publications are solely those of the individual author(s) and contributor(s) and not of MDPI and/or the editor(s). MDPI and/or the editor(s) disclaim responsibility for any injury to people or property resulting from any ideas, methods, instructions or products referred to in the content.